



## Removal of phosphate from aqueous solution by magnetic Fe–Zr binary oxide

Fei Long<sup>a,b</sup>, Ji-Lai Gong<sup>a,b,c,\*</sup>, Guang-Ming Zeng<sup>a,b</sup>, Long Chen<sup>a,b</sup>, Xi-Yang Wang<sup>a,b</sup>, Jiu-Hua Deng<sup>a,b</sup>, Qiu-Ya Niu<sup>a,b</sup>, Hui-Ying Zhang<sup>a,b</sup>, Xiu-Rong Zhang<sup>a,b</sup>

<sup>a</sup> College of Environmental Science and Engineering, Hunan University, Lushan South Road, Changsha, Hunan 410082, PR China

<sup>b</sup> Key Laboratory of Environmental Biology and Pollution Control, Hunan University, Ministry of Education, Changsha 410082, PR China

<sup>c</sup> State Key Laboratory of Chemo/Biosensing and Chemometrics, Hunan University, Changsha 410082, PR China

### ARTICLE INFO

#### Article history:

Received 6 January 2011

Received in revised form 28 March 2011

Accepted 30 March 2011

#### Keywords:

Magnetic  
Fe–Zr binary oxide  
Adsorption  
Phosphate

### ABSTRACT

Phosphorus removal was a crucial aspect in controlling eutrophication problem of water pollution. Zirconium oxide was a suitable adsorbent for phosphate removal due to its good adsorption efficiency, but it suffered from the separation inconvenience. In this paper, magnetic Fe–Zr binary oxide was synthesized and used as adsorbent for removing phosphate from aqueous solution. The adsorbent was characterized by energy dispersive analysis system of X-ray, scanning electron microscopy (SEM), infrared spectrum (IR), X-ray powder diffraction (XRD) analysis and BET surface area measurements. The results showed that kinetic data followed a pseudo-second-order model and equilibrium data were well fitted by the Langmuir model. The maximum adsorption capacity was 13.65 mg P/g at pH 4. The adsorption mechanism was mainly derived from ion-exchange of zirconium species and partly originated from magnetite species of Fe–Zr binary oxide. The main advantages of magnetic Fe–Zr binary oxide adsorbent consisted in its separation convenience and highly efficient reusability compared to the other adsorbents.

Crown Copyright © 2011 Published by Elsevier B.V. All rights reserved.

### 1. Introduction

Phosphorus, as an essential resource and material, is widely used in the areas of agriculture and industry. However, a large amount of phosphate promotes the growth of the alga due to its extensive use. Some algae are toxic, which lead to the disturbance of organisms balance in water. The rapid depletion of dissolved oxygen level makes the fish and other aquatic life dead when the algae decay. Therefore, phosphorus has a great impact on the lakes, rivers and seas which people depend on [1]. It is of significant importance to control the amounts of phosphorous in water to maintain a green environment for the forthcoming generation [2].

There are mainly three kinds of methods to remove phosphate including chemical precipitation, biological treatment, and adsorption [3]. Chemical precipitation method was first used to resolve the problem of rich nutritional pollution. It was also applied in treating industrial wastewater containing high concentration of phosphate. Moreover, this method could produce high-quality of phosphate precipitates such as struvite. However, the cost was expensive and the recovery of phosphorus from chemical sludge was very difficult [4]. Biological treatment was widely used in the removal

of organophosphorous chemicals in food and domestic wastewater. People utilized polyphosphate accumulative organisms (PAOs) or plants assimilating phosphate to reduce the phosphorous concentration. Nevertheless, this method had disadvantages of slow treatment speed, complex operation process and requiring considerable infrastructure investment. Furthermore, it was unsuitable for treating wastewater containing high concentration of phosphate [5].

Adsorption methodology could overcome the problems existed in chemical precipitation and biological treatment. Adsorption method was found to be superior to above techniques for removal of pollutants from aqueous solution in terms of flexibility and simplicity of design, ease of operation and insensitivity to toxic pollutants. It also did not result in the formation of harmful substances [6]. It was well known that the adsorption capacity and efficiency were greatly dependent on the materials of adsorbents.

Many materials for removal of phosphate were used as adsorbents in the literatures including fly ash [7–9], red mud [10–12], slag [13–15], sand [16,17], aluminum hydroxide [18–20], iron oxide [21–23], calcium based adsorbents [24,25], niobium oxide [26], calcite [1] and peat [27].

In addition, zirconium oxide was also a suitable adsorbent for phosphate removal due to its good efficiency of absorption and desorption for recycling [28]. Zirconia was one of the ceramic oxides and was used to adsorb arsenate and phosphate [29,30]. Biswas et al. reported orange waste gel loaded with zirconium for removal of phosphorus from water [31]. Liu et al. also reported mesoporous

\* Corresponding author at: College of Environmental Science and Engineering, Hunan University, Lushan South Road, Changsha, Hunan 410082, PR China.  
Tel.: +86 731 88822829; fax: +86 731 88822829.

E-mail address: [jilgong@gmail.com](mailto:jilgong@gmail.com) (J.-L. Gong).

ZrO<sub>2</sub> for phosphate removal [30]. However, both of them suffered from the drawback of separation inconvenience. They could overcome the drawback described above if the adsorbents were magnetic. The reason was that they could be easily separated using magnet and desorbed for reuse [32,33]. To our knowledge, the use of zirconium oxide with magnetic property as adsorbent for phosphate removal was quite rare.

In this paper, we synthesized magnetic Fe–Zr binary oxide and used it as adsorbent for removal of phosphate from aqueous solution. The adsorbent in our work could be easily collected with a high gradient magnet. The magnetic Fe–Zr binary oxide adsorbent possessed favorable adsorption capacity for phosphate and exhibited good regeneration property. Experimental parameters such as the effect of pH, contact time, ionic strength and effect of other anions were also investigated.

## 2. Materials and methods

### 2.1. Materials

#### 2.1.1. Chemicals

Zirconyl chloride (ZrOCl<sub>2</sub>·8H<sub>2</sub>O), ferrous chloride (FeCl<sub>2</sub>·4H<sub>2</sub>O), polyvinyl alcohol (PVA), hydrogen peroxide (H<sub>2</sub>O<sub>2</sub>), anhydrous potassium dihydrogen orthophosphate (KH<sub>2</sub>PO<sub>4</sub>), ascorbic acid and ammonium molybdate were purchased from Shenzhen Nanopoint Company (Shenzhen, China). The standard phosphate solution was prepared by dissolving KH<sub>2</sub>PO<sub>4</sub> in appropriate amounts of distilled water and the KH<sub>2</sub>PO<sub>4</sub> should be first dried for 2 h at 110 °C. The pH values of solutions were adjusted with NaOH and HCl. All reagents were of analytical grade. Distilled water was used through all the experiments, and the experiments were performed twice.

#### 2.1.2. Synthesis of magnetic materials

The synthesis of magnetic Fe–Zr binary oxide was performed with the modification of the previous literature [34]. First, the amount of 15 g zirconyl chloride and 90 mL of 0.24 M ferrous chloride were added into 120 mL 5% PVA solution in a three necked round bottom flask. Then, the mixture was mechanically stirred under a 50 °C water bath for 10 min followed by the addition of 30 mL 0.24 M H<sub>2</sub>O<sub>2</sub>. Subsequently, the amount of 120 mL 3 M NaOH was quickly injected into the flask. The reaction was continued for 2 h. After the reaction completed, the black product was collected by magnet and washed to neutral with plenty of water in order to remove the Cl<sup>-</sup> and OH<sup>-</sup> consisted in the solution. The product was dried at 80 °C for 18 h. Then, the dried product was transferred into muffle furnace and kept at 500 °C for 4 h. Finally, the obtained Fe–Zr binary oxide adsorbent was cooled at room temperature and kept at desiccator for further use.

### 2.2. Adsorbent characterization

The sample composition and element contents were analyzed by energy dispersive analysis system of X-ray (EDAX) using EDX-GENESIS (EDAX, Ltd., USA). The surface morphology of the prepared adsorbent was observed by scanning electron microscopy (SEM) using a JSM-6700F LV microscope. The component of the synthesized magnetic material was characterized by Rigaku TTRIII X-ray diffraction patterns recorded on a D/max 2550 X-ray diffractometer (Rigaku, Japan) using Cu K $\alpha$  radiation ( $\lambda = 0.1541$  nm). The magnetic properties were measured by magnetization curves using a HH-50 vibrating sample magnetometer in the condition of sensitivity 20 mV. The Brunauer–Emmett–Teller (BET) specific surface area and the pore size distribution were analyzed by nitrogen adsorption–desorption measurements through a Monosorb direct reading specific surface analyzer (Quantachrome Co., USA).

The IR spectra of the magnetic material before and after phosphate adsorption were measured by a Fourier transform infrared spectrometer (FTIR, WQF-410, Beijing Second Optical Instrument Factory, China). And the zeta potential of Fe–Zr binary oxide suspension was determined by a Zeta Meter 3.0 (Zeta Meter Inc.) equipped with a microprocessor unit.

### 2.3. Adsorption experiment

The adsorption experiments of phosphate were performed according to the batch method. All the Erlenmeyer flasks containing appropriate amount of adsorbent and phosphate solution were placed on a constant temperature bath oscillator to vibrate at room temperature (25 °C). After a period of time, the adsorbent was separated from the solution using a permanent magnet and the initial and final phosphate concentrations were determined using the ammonium molybdate spectrophotometric method.

#### 2.3.1. Effect of contact time

The effect of contact time on each sorption was investigated in different time intervals ranging from 5 min to 2 days with initial phosphate concentration of 50 mg P/L. The amount of 0.2 g Fe–Zr binary oxide was added into 200 mL of KH<sub>2</sub>PO<sub>4</sub> solution. After the completion of the reaction, the amount of 1 mL mixture was taken out from each flask and the magnetic adsorbent was separated followed by the determination of the residual phosphate concentrations. The adsorption kinetic experiments were carried out at pH 4.

#### 2.3.2. Adsorption isotherm

Adsorption experiments were performed in 50 mL glass Erlenmeyer flasks containing 25 mL of different initial concentrations from 0 to 100 mg P/L and 1 g/L of Fe–Zr binary oxide at fixed pH 4.0. The contact time was 24 h.

#### 2.3.3. Effect of pH and ionic strength

To gain further insight into the adsorption process, the influence of pH and ionic strength were studied as follows. Solutions containing 50 mg P/L of phosphate and known concentrations of NaCl (0.1 M, 0.01 M and 0.001 M) were adjusted with HCl and NaOH solutions to the desired pH values from 3 to 11. The adsorbent dosage and reaction time was 1 g/L and 24 h, respectively.

#### 2.3.4. Effect of coexisting anion

The effects of nitrate, sulfate, acetic and citrate on the adsorbed phosphate were investigated. Two kinds of anion concentration (0.001 M and 0.01 M) were also investigated. The initial phosphate concentration, pH value and adsorbent dosage were 50 mg P/L, 4 and 1 g/L, respectively. The other conditions were the same as mentioned above.

#### 2.3.5. Desorption and reusability

For estimating the regeneration of the Fe–Zr binary oxide adsorbent, desorption experiments were conducted using four different concentrations of NaOH solutions. The Fe–Zr binary oxide adsorbent was first saturated with phosphate for 24 h and separated from the solution. Then it was immersed in different NaOH solutions (0.01, 0.1, 0.5 and 1 M) for another 24 h. The initial phosphate concentration and adsorbent dosage were 50 mg P/L and 1 g/L, respectively. The residual phosphate concentrations after adsorption and after desorption should both be determined to calculate the desorption percentage. The other conditions were the same as mentioned above.

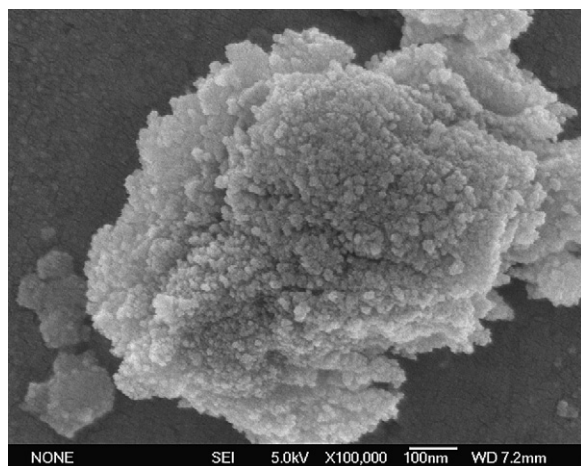


Fig. 1. SEM of the magnetic Fe–Zr binary oxides.

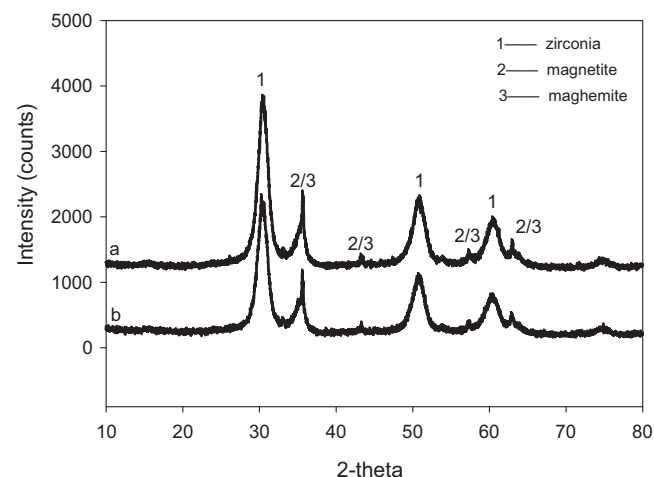


Fig. 3. XRD patterns of magnetic Fe–Zr binary oxides before treatment (a) and after treatment (b).

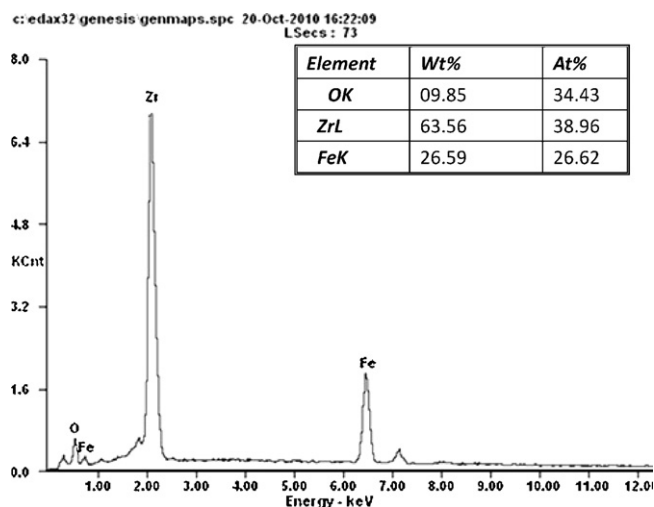


Fig. 2. EDAX spectrum of the magnetic adsorbents using 15 g zirconyl chloride during synthesis.

Finally, 0.1M NaOH was chosen to repeat above processes of adsorption and desorption for investigating the regeneration capacity of the Fe–Zr binary oxide adsorbent.

### 3. Results and discussion

#### 3.1. Characterization of synthesized magnetic materials

The SEM image of the Fe–Zr binary oxide was shown in Fig. 1. The surface of Fe–Zr binary oxide was uneven and rough with abundant protuberances and lots of pores, which favored the diffusion of the phosphate to its surface.

X-ray energy dispersive analysis experiments were performed to characterize magnetic product composition and element contents (see Fig. 2). It was observed that the concentrations of zirconium and iron elements were 38.96% and 26.62%, respectively. The Zr/Fe molar ratio was 2.16.

The XRD patterns of the Fe–Zr binary oxide before and after adsorption tests were demonstrated in Fig. 3. It was observed that the three strongest peaks ( $2\theta = 30.4^\circ$ ,  $50.8^\circ$  and  $60.4^\circ$ ) could be assigned to zirconia [28], and the reflection ( $2\theta = 35.6^\circ$ ,  $43.2^\circ$ ,  $57.3^\circ$  and  $62.9^\circ$ ) could be assigned to magnetite ( $\text{Fe}_3\text{O}_4$ ) and maghemite ( $\text{Fe}_2\text{O}_3$ ) [35]. These results indicated that the principal components of magnetic Fe–Zr binary oxide adsorbent were zirconia, magnetite

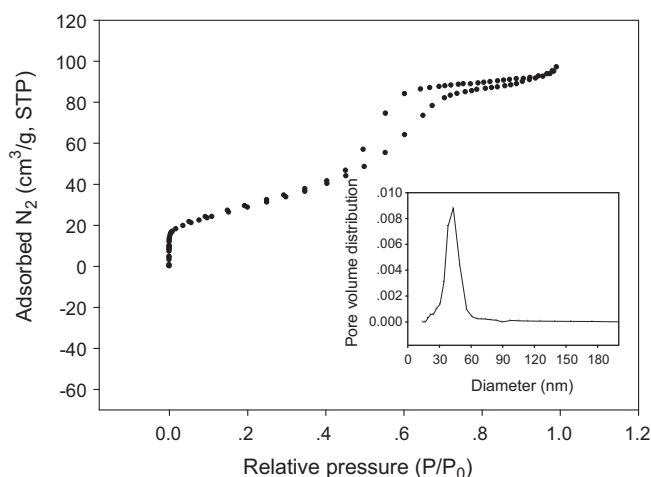


Fig. 4. Changes in  $\text{N}_2$  gas adsorption/desorption isotherm of Fe–Zr binary oxide.

and maghemite. Among them, the magnetite and maghemite were magnetic, which proved that the magnetic material was a composite of Fe oxide and Zr oxide. No obvious change can be found about Fe–Zr binary oxide before and after phosphate adsorption. Therefore, it revealed that crystalline phase of Fe–Zr binary oxide remained unchanged even after phosphate adsorption.

The saturated magnetization of Fe–Zr binary oxide adsorbent was 6.1 emu/g and the results were shown in Fig. S1. Compared with the saturated magnetization values (4.36 and 1.97 emu/g) reported in previous literatures [36,37], the magnetic of Fe–Zr binary oxide adsorbent was large enough to be collected by the high gradient magnet.

The BET surface area of Fe–Zr binary oxide adsorbent was  $106.2 \text{ m}^2/\text{g}$  (Fig. 4). The hysteresis observed at higher relative pressures ( $>0.5$ ) indicated that lots of mesopores were present on the surface of Fe–Zr binary oxide adsorbent [28].

The changes of vibration frequency about adsorbent were determined by the FTIR spectrometry and the results were shown in Fig. 5. A strong and broad band in  $3600\text{--}3100 \text{ cm}^{-1}$  region (O–H stretching vibration) should be assigned for the presence of hydroxyl of coordinate water molecules [38]. Compared with spectrum of Fe–Zr binary oxide before phosphate adsorption (Fig. 5(a)), the peaks of  $1618 \text{ cm}^{-1}$  (O–H bending vibration) and  $1336 \text{ cm}^{-1}$  (O–H bending vibration) after phosphate adsorption (Fig. 5(b)) were weakened dramatically and completely disappeared, respec-

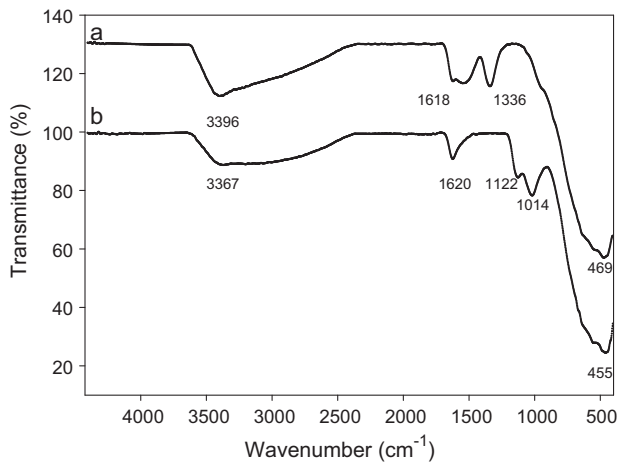


Fig. 5. FTIR of magnetic Fe–Zr binary oxides before treatment (a) and after treatment (b).

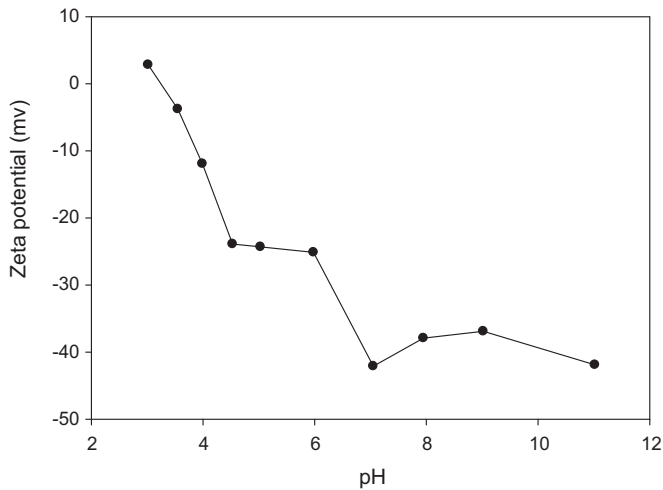


Fig. 6. Plot of zeta potential of magnetic Fe–Zr binary oxides as a function of pH in 0.01 M NaCl at 25 °C.

tively. And the new peak appearing at  $1014\text{ cm}^{-1}$  was attributed to the bending vibration of adsorbed phosphate accompanied by a new weaker shoulder peak appearing at  $1122\text{ cm}^{-1}$  (Fig. 5(b)) [28]. These results proved that phosphate was successfully adsorbed on the surface of Fe–Zr binary oxide adsorbent and the hydroxyl of Fe–Zr binary oxide adsorbent was disappeared simultaneously. Therefore, it was suggested that the adsorption mechanism between Fe–Zr binary oxide adsorbent and the phosphate may result from the ion exchange between the hydroxyl on the adsorbent surface and phosphate in the solution. The bands of 455 and  $469\text{ cm}^{-1}$  observed in samples were due to metal oxygen stretching vibration [38]. It could be assigned to the Fe oxygen stretching vibration in this magnetic material. And the shift observed for the samples might be caused by the difference of Fe–Zr binary oxide adsorbent between before and after phosphate adsorption.

Fig. 6 showed zeta potential of Fe–Zr binary oxide adsorbent in different pH values ranging from 3 to 11. The results showed that the isoelectric point of the adsorbent was at pH 3.24. The surface of adsorbent was positive when pH value was below 3.24. While pH value was above 3.24, the charge of the magnetic adsorbent was negative.

### 3.2. Effect of contact time

In order to further understand the characteristics of the absorption process, the pseudo-first-order adsorption, pseudo-second-order, and intra-particle diffusion models were applied to fit experimental data obtained from batch experiments.

A pseudo-first-order kinetic model is given as following equation,

$$\log(q_e - q_t) = \log q_e - \frac{k_1 t}{2.303} \quad (\text{A.1})$$

A pseudo-second-order kinetic model is also analyzed to fit the data and showing as following equation,

$$\frac{t}{q_t} = \frac{1}{k_2 q_e^2} = \frac{t}{q_e} \quad (\text{A.2})$$

The intra-particle diffusion model is usually described by the following equation.

$$q_e = k_p t^{0.5} + C \quad (\text{A.3})$$

where  $q_e$  and  $q_t$  is the amounts of phosphate adsorbed on per unit Fe–Zr binary oxide at equilibrium and at time  $t$ , respectively (mg P/g),  $k_1$  is the pseudo-first-order rate constant for the adsorption process and can be obtained from the plots of  $\log(q_e - q_t)$  against  $t$ ,  $k_2$  is the pseudo-second-order rate constant for the adsorption process and can be obtained from the plots of  $t/q_t$  against  $t$ ,  $k_p$  is the intra-particle diffusion rate constant and can be obtained from the slope of straight-line portions of plot of  $q_t$  against  $t^{1/2}$ , and  $C$  is a constant gained from the intercept of plot of  $q_t$  against  $t^{1/2}$ .

As shown in Fig. 7(a), the amounts of phosphate on the adsorbent were measured in different contact time. The result showed that the process of adsorption kinetics took place in two opposite steps: a rather fast uptake of the phosphate occurs and about 86% of phosphates were adsorbed within the first 2 h. The first step was followed by a slow stage until the equilibrium state was reached. It was observed that the phosphate adsorption almost reached equilibrium after 24 h. Therefore, the equilibrium time of 24 h was chosen for further experiment.

The results of linear forms of pseudo-first-order, pseudo-second-order and intra-particle diffusion kinetic models on the experiment data were presented in Fig. 7(b), (c) and (d), respectively. The value of correlation coefficient ( $R=0.9993$ ) was far closer to 1 than the values of pseudo-first-order and intra-particle diffusion kinetic models (the correlation coefficient values of which were 0.9452 and 0.9636, respectively). Therefore, the pseudo-second-order model was fitted well with our experiment data indicating that the rate-limiting step for removal phosphate by Fe–Zr binary oxide adsorbent may be the chemical adsorption [39].

The adsorption process was essentially divided into two or more steps: the first step was the external surface adsorption or instantaneous adsorption stage. The second step was the gradual adsorption stage, where the adsorption rate was limited by intra-particle diffusion. In some cases, the third step was the final equilibrium stage when the intra-particle diffusion started to shut down [40]. The linear of  $Q_e$  against  $t^{1/2}$  in Fig. 7(d) showed that adsorption process was obviously divided into three steps. The first linear step (before 2 h) was a very fast stage. The reason may be that the phosphate was quickly transported to the surface of adsorbent under the concentration gradient force. The second linear step (from 2 h to 24 h) was the gradual adsorption process where intra-particle diffusion started to limit the rate of adsorption. The third linear step (after 24 h) was the equilibrium stage, where the adsorption sites of the adsorbent surface were saturated and the intra-particle diffusion of adsorption was shut down. Therefore, the magnetic material in our work could be used to adsorb phosphate if the adsorption time was less than 2 h.

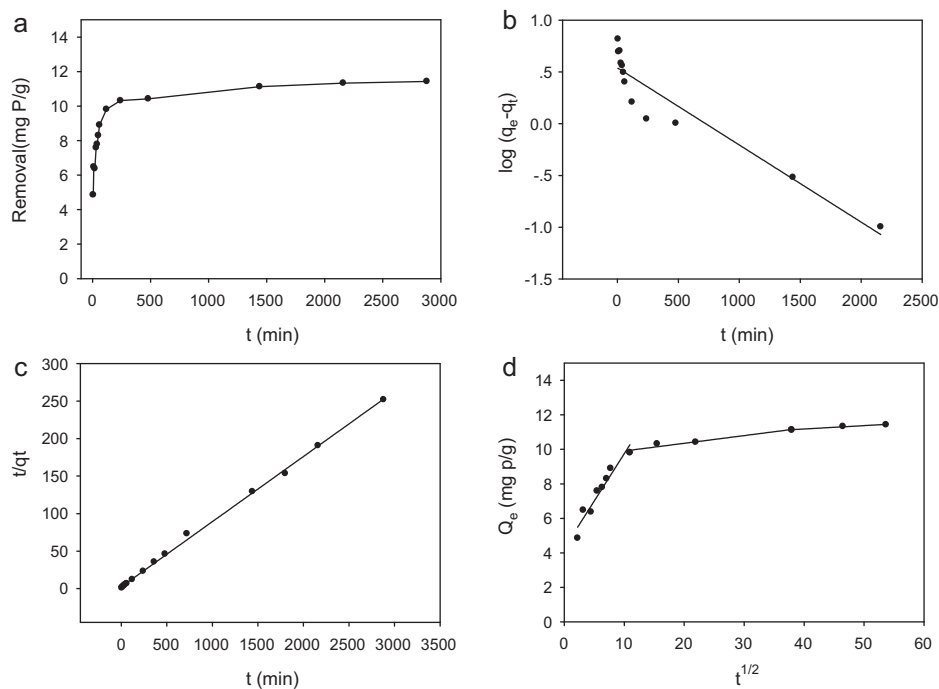


**Fig. 7.** The influence of contact time on the amount of phosphate absorption by magnetic Fe–Zr binary oxides (a), the pseudo-first-order kinetic model (b), the pseudo-second-order kinetic model (c), and intra-particle diffusion plots for phosphate adsorption onto magnetic Fe–Zr binary oxides (d).

### 3.3. Adsorption isotherm

Langmuir and Freundlich models were used to describe the adsorption capacity of Fe–Zr binary oxide for phosphate. Langmuir model was appropriate for monolayer adsorption onto the surface of adsorbent. All the adsorption sites were equal and the number of identical sites limited the adsorption capacity. It can be shown as below.

$$\frac{C_e}{q_e} = \frac{C_e}{q_{\max}} + \frac{1}{K_L q_{\max}} \quad (\text{B.1})$$

According to Freundlich model, it was often applicable to describe the models of multilayer adsorption onto the surface of heterogeneous sites with different bond energy. The equation of Freundlich model is given as following.

$$\log q_e = \log K_F + \frac{1}{n} \log C_e \quad (\text{B.2})$$

where  $q_e$  and  $q_{\max}$  is the amount and the maximum amount of adsorbed phosphate per unit weight of adsorbent (mg P/g), respectively,  $C_e$  is the residual concentration of adsorbate in bulk solution (mg P/L),  $K_L$  is a constant determined by plotting  $C_e/q_e$  versus  $C_e$ ,  $K_F$  and  $1/n$  are the constants related to adsorption of adsorbent and intensity of the adsorption, respectively.

As demonstrated in Fig. 8, the experimental data were fitted better with Langmuir model ( $R=0.9856$ ) compared with the Freundlich model ( $R=0.9799$ ). The calculated maximum adsorption capacity was 13.65 mg P/g which was much higher than those adsorbents had been reported, such as iron oxide tailing (12.6 mg P/g) [21], peat (8.91 mg P/g) [27], La doped vesuvianite (6.7 mg P/g) [41], Fe–Mn binary oxide (11.7 mg P/g) [42] and MgMn layered double hydroxides (7.3 mg P/g) [43]. Moreover, the adsorption capacity of Fe–Zr binary oxide toward phosphate in this work was comparable to that of other adsorbents such as Fe-EDA-SAMMS (14.2 mg P/g) [3], hydroxy niobium oxide (15 mg P/g) [26] and La/Al pillared montmorillonite (13.0 mg P/g) [44]. It was noticed that the adsorption capacity was negligible when the pure iron oxide without the component of zirconium was used as adsorbent in our experiments.

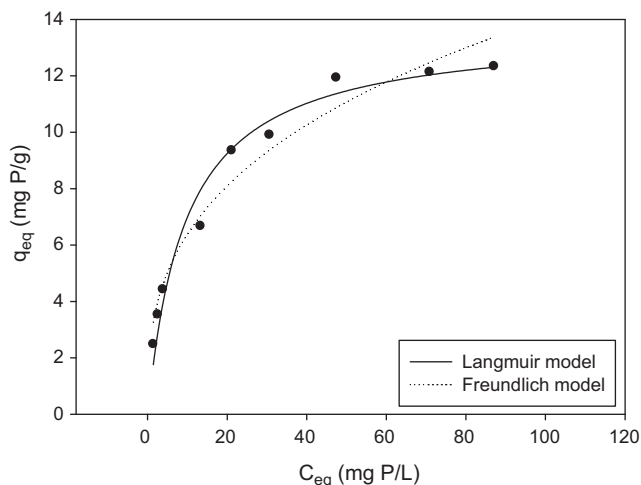


**Fig. 8.** Adsorption isotherm for phosphate on magnetic Fe–Zr binary oxides at pH 4.

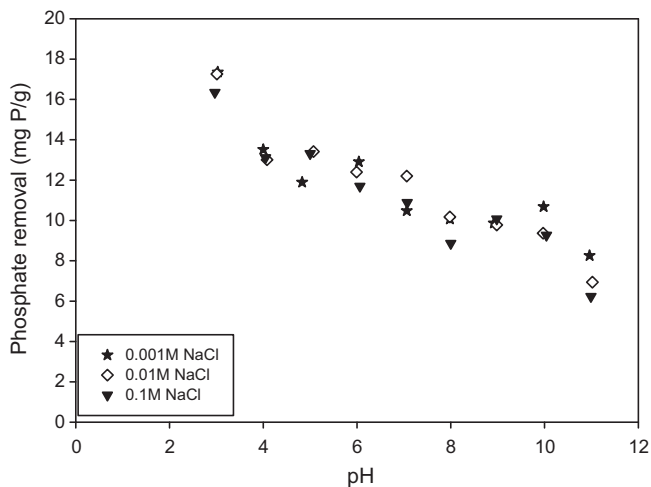
Therefore, the adsorption of phosphate was mainly contributed to zirconium oxide.

The capacity of Fe–Zr binary oxide adsorbent was much worse than that of mesoporous  $\text{ZrO}_2$  (29.7 mg P/g) [28]. This phenomenon was partly caused by the lower proportion of  $\text{ZrO}_2$  in our magnetic material than the pure one.

The Zr/Fe molar ratio of the magnetic adsorbent is important for phosphate removal. The Zr/Fe molar ratios of adsorbents prepared using different amounts of zirconyl chloride ranging from 6 g to 24 g during synthesis were analyzed by EDAX spectra (see Fig. S2). The saturated magnetization curves of adsorbents containing different Zr/Fe molar ratios were shown in Fig. S1. The Zr/Fe molar ratios of adsorbents in the starting before synthesis and in the final product were listed in Table 1 along with their adsorption capacities and saturated magnetization data. Obviously, the Zr/Fe molar ratios increased with the increase of zirconyl chloride amounts during

**Table 1**The Zr/Fe molar ratios, adsorption capacities and saturation magnetization of adsorbents prepared using different amounts of ZrOCl<sub>2</sub> during synthesis.

Amounts of ZrOCl <sub>2</sub> added (g)	Zr/Fe mole ratio in the starting	Zr/Fe molar ratio in product	Adsorption capacity (mg P/g)	Saturated magnetization (emu/g)
0.00	0.00	0.00	1.16	41.99
6.00	0.86:1	0.52:1	10.21	16.45
9.00	1.30:1	0.86:1	11.70	14.93
15.00	2.16:1	1.46:1	13.65	6.10
21.00	3.02:1	1.79:1	14.64	4.13
24.00	3.45:1	2.16:1	14.95	1.02

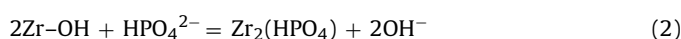
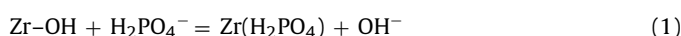
**Fig. 9.** Effect of pH and ionic strength on phosphate absorption by magnetic Fe–Zr binary oxides.

synthesis followed by the increase of adsorption capacities toward phosphate and the decrease of saturated magnetization. The reason that adsorption capacities increased with the increase of Zr/Fe molar ratios was attributed to the increased zirconium species in Fe–Zr binary oxide adsorbents. Nevertheless, saturated magnetization of Fe–Zr binary oxide adsorbents decreased as a result of the decreased proportion of magnetic species in adsorbents. It was found that the prepared adsorbents exhibited very low or even negligible magnetic properties when the Zr/Fe molar ratios were greater than 3.02:1 in the starting. Therefore, the Zr/Fe molar ratio of 3.02:1 in the starting was selected to prepare Fe–Zr binary oxide adsorbent. Additionally, the Zr/Fe molar ratio in Fe–Zr binary oxide products was lower compared to that in the starting indicating part of zirconyl chloride failure to form Fe–Zr binary oxide.

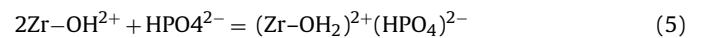
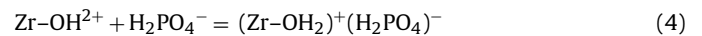
Noticeably, the adsorption capacity of Fe–Zr binary oxide adsorbent toward phosphate was 1.16 mg P/g in the absence of zirconyl chloride during synthesis. It revealed that the phosphate adsorption was partly derived from magnetite species in Fe–Zr binary oxide adsorbent.

#### 3.4. Effect of pH and ionic strength

The effects of pH and ionic strength on phosphate adsorption were shown in Fig. 9. The results indicated that the pH was a significant parameter controlling the process of adsorption, while the ionic strength had a little influence. The phosphate uptake obviously increased with the decrease of pH, which should be attributed to the competition between hydroxyl ions and the phosphate ions on the surface of the adsorbent [28]. It was reported that the adsorption process was based on the ion-exchange mechanism as follows:



When the pH is lower than the isoelectric point



Obviously, the concentration of hydroxyl ions promoted the opposite reactions described above leading to the decrease of phosphate adsorption at higher pH solution. Therefore, adsorption reaction was much favorable at lower pH than at higher pH value. It was observed that the adsorption capacity could reach 17.87 mg P/g at pH 3. As a result, the Fe–Zr binary oxide could be well used to adsorb phosphate in the acidic environment.

Noticeably, we found that the final pH of solution was higher after the adsorption process (shown in Table 2), which indicated that hydroxyl ion released into the final solution after uptake phosphate onto the surface of Fe–Zr binary oxide adsorbent. Therefore, combining IR data and adsorption result in the absence of zirconium species described above, we could confirm that the adsorption essence toward phosphate was mainly derived from ion-exchange mechanism of zirconium species and partly originated from magnetite species in Fe–Zr binary oxide adsorbent.

When the pH was below the isoelectric point (pH = 3.24), the protonated process occurred and the surface of materials was the positive charge leading to static electricity force between positive material and negative phosphate ions. Therefore, the reason that the much higher capacity at pH 3 was observed in contrast to pH 4 was due to the electrostatic force besides interaction of ion-exchange.

Simultaneously, it had a little influence on the removal of phosphate by Fe–Zr binary oxide with different concentrations of ionic strength shown in Fig. 9. It meant that Fe–Zr binary oxide could be used as adsorbent to remove phosphate from high salinity wastewater.

#### 3.5. Effects of coexisting anion

Natural water and wastewater always contained lots of coexisting anions, which could potentially compete with phosphate for the adsorption sites. Thus, the interferences of coexisting anions, including nitrate, sulfate, citrate and acetic were studied. The results (shown in Table 2) demonstrated that the amount of adsorbed phosphate decreased in the presence of nitrate, sulfate and citrate. The interference of citrate on phosphate adsorption was much more obvious than that of nitrate and sulfate. This may be due to the competition between the phosphate and hydroxyl groups of citrate. However, the amount of adsorbed phosphate increased in the presence of acetic which may be caused by the lower final pH of sodium acetic solution. It was described above that lower pH favored phosphate adsorption. Furthermore, the interferences were much more obvious at the higher concentrations of coexisting anions compared with that at the lower concentrations.

**Table 2**  
Effects of coexisting anions on phosphate removal by magnetic Fe–Zr binary oxides at initial pH 4.

Matrix	Final pH	Amount of phosphate removed (mg P/g)	Matrix	Final pH	Amount of phosphate removed (mg P/g)
Phosphate only	6.54	12.39			
+0.01 M sodium nitrate	6.33	10.98	+0.001 M sodium nitrate	6.47	12.04
+0.01 M sodium sulfate	6.18	11.03	+0.001 M sodium sulfate	6.47	11.08
+0.01 M sodium citrate	4.05	7.23	+0.001 M sodium citrate	4.69	9.36
+0.01 M sodium acetic	4.10	13.66	+0.001 M sodium acetic	4.85	12.64

**Table 3**  
The desorption of phosphate from magnetic Fe–Zr binary oxides with NaOH solution.

NaOH concentration (M)	0.01	0.1	0.5	1
Desorbed percentage (%)	54.3	72.8	73.7	74.5

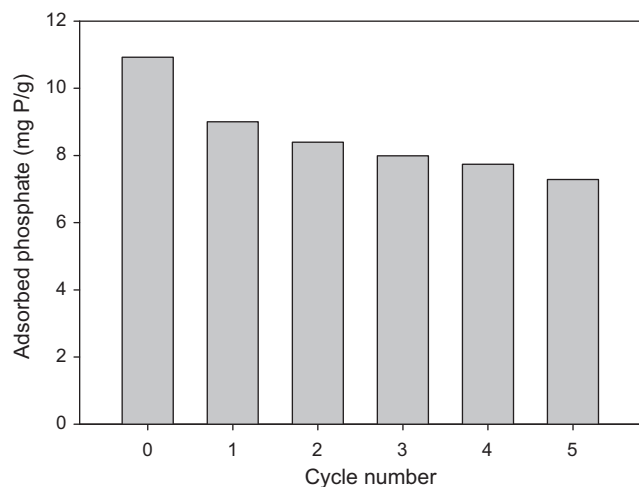


**Fig. 10.** Reusability of magnetic Fe–Zr binary oxides regenerated by 0.1 M NaOH.

### 3.6. Desorption and reusability

Due to the adsorption capacities decreased with the increase of pH, different concentrations of NaOH solution were used to investigate the desorption process. The results were listed in Table 3. It was discovered that the desorbed phosphate increased with the increasing concentration of NaOH. The phosphate desorption percentages were 54.3%, 72.8%, 73.7% and 74.5%, when the concentrations of NaOH solution were 0.01 M, 0.1 M, 0.5 M and 1 M, respectively. Therefore, 0.1 M NaOH solution was selected as an eluent to desorb phosphate from the surface of Fe–Zr binary oxide adsorbent.

The adsorption–regeneration cycles were carried out five times. The relationship between cycle number and adsorption capacity was shown in Fig. 10. The value of cycle 0 was assigned to the adsorption capacity of the original Fe–Zr binary oxide. In general, the adsorption capacity decreased with the increase of the cycle number. The amount of decrease for the first regeneration cycle was about 83% of the original adsorption capacity. Moreover, when the fifth cycle was over, the adsorption capacity could also reach 66.7% of the original one. It sufficiently displayed the good regeneration results for the magnetic Fe–Zr binary oxide.

## 4. Conclusion

The results suggested that the magnetic Fe–Zr binary oxide could be successfully applied for adsorbing phosphate and controlling the phosphorous pollution in aqueous solution. The effects of contact time, initial phosphate ions concentrations, pH and ionic strength on the adsorption process were discussed. The conclusions were showing as follows:

- (1) The adsorbent possessed a rough surface and many mesoporous pores. Its specific surface area and  $\text{pH}_{\text{ZPC}}$  was 106.2  $\text{m}^2/\text{g}$  and 3.24, respectively.
- (2) The kinetic data were well fitted with pseudo second-order model. The adsorption isotherm described by Langmuir model was better than Freundlich model. The maximum adsorption capacity was 13.65 mg P/g at pH 4.
- (3) Phosphate adsorption capacity decreased with the increase of pH ranging from 3 to 11. The adsorption mechanism was due to the ion exchange between hydroxyl and phosphate.
- (4) The magnetic Fe–Zr binary oxide adsorbent could be regenerated using 0.1 M NaOH solution as eluant. The adsorption capacity was able to reach up to 66.7% of the original adsorption capacity after the fifth cycle.
- (5) The magnetic Fe–Zr binary oxide adsorbent with saturation magnetization of 6.1 emu/g could be easily separated with a high gradient magnet. Therefore, it could be a potential material for the phosphate removal.

## Acknowledgements

The authors are grateful for the financial supports from National Natural science Foundation of China (50808070, 50978088, 51039001), the program for New Century Excellent Talents in University from the Ministry of Education of China (NCET-09-0328), the Postdoctoral Science Foundation of China (20070410301, 200902468), the Specialized Research Fund for the Doctoral Program of Higher Education (20070532059), the Program for Changjiang Scholars and Innovative Research Team in University (IRT0719), Hunan Provincial Natural Science Foundation of China (08JJ4006, 10JJ7005), the Xiangjiang Water Environmental Pollution Control Project subjected to the National Key Science and Technology Project for Water Environmental Pollution Control (2009ZX07212-001-02 and 2009ZX07212-001-06) and the Hunan Key Scientific Research Project (2009FJ1010).

## Appendix A. Supplementary data

Supplementary data associated with this article can be found, in the online version, at [doi:10.1016/j.cej.2011.03.102](https://doi.org/10.1016/j.cej.2011.03.102).

## References

- [1] K. Karageorgiou, M. Paschalis, G.N. Anastassakis, Removal of phosphate species from solution by adsorption onto calcite used as natural adsorbent, *J. Hazard. Mater.* 139 (2007) 447–452.
- [2] D.P. Van Vuuren, A.F. Bouwman, A.H.W. Beusen, Phosphorus demand for the 970–2100 period: a scenario analysis of resource depletion, *Global Environ. Change* 20 (2010) 428–439.
- [3] W. Chouyyok, R.J. Wiacek, K. Pattamakomsan, T. Sangvanich, R.M. Grudzien, Phosphate removal by anion binding on functionalized nanoporous sorbents, *Environ. Sci. Technol.* 44 (2010) 3073–3078.
- [4] X. Cheng, X.R. Huang, X.Z. Wang, B.Q. Zhao, A. Chen, D. Sun, Phosphate adsorption from sewage sludge filtrate using zinc–aluminum layered double hydroxides, *J. Hazard. Mater.* 169 (2009) 958–964.
- [5] J.C. Liu, Warmadewanthi, C.J. Chang, Precipitation flotation of phosphate from water, *Colloids Surf. A* 347 (2009) 215–219.
- [6] M. Rafatullah, O. Sulaiman, R. Hashim, A. Ahmad, Adsorption of methylene blue on low-cost adsorbents: a review, *J. Hazard. Mater.* 177 (2010) 70–80.

- [7] S.G. Lu, S.Q. Bai, L. Zhu, H.D. Shan, Removal mechanism of phosphate from aqueous solution by fly ash, *J. Hazard. Mater.* 161 (2009) 95–101.
- [8] P. Pengthamkeerati, T. Satapanajaru, P. Chularuengsookorn, Chemical modification of coal fly ash for the removal of phosphate from aqueous solution, *Fuel* 87 (2008) 2469–2476.
- [9] K. Xu, T. Deng, J.T. Liu, W.G. Peng, Study on the phosphate removal from aqueous solution using modified fly ash, *Fuel* 89 (2010) 3668–3674.
- [10] Y. Zhao, J. Wang, Z.K. Luan, X.J. Peng, Z. Liang, L. Shi, Removal of phosphate from aqueous solution by red mud using a factorial design, *J. Hazard. Mater.* 165 (2009) 1193–1199.
- [11] W.W. Huang, S.B. Wang, Z.H. Zhu, L. Li, X.D. Yao, V. Rudolph, F. Haghseresh, Phosphate removal from wastewater using red mud, *J. Hazard. Mater.* 158 (2008) 35–42.
- [12] Q.Y. Yue, Y.Q. Zhao, Q. Li, W.H. Li, B.Y. Gao, S.X. Han, Y.F. Qi, H. Yu, Research on the characteristics of red mud granular adsorbents (RMGA) for phosphate removal, *J. Hazard. Mater.* 176 (2010) 741–748.
- [13] Y.J. Xue, H.B. Hou, S.J. Zhu, Characteristics and mechanisms of phosphate adsorption onto basic oxygen furnace slag, *J. Hazard. Mater.* 162 (2009) 973–980.
- [14] J.B. Xiong, Z.L. He, Q. Mahmood, D. Liu, X.E. Yang, E. Islam, Phosphate removal from solution using steel slag through magnetic separation, *J. Hazard. Mater.* 152 (2008) 211–215.
- [15] J. Yang, S. Wang, Z.B. Lu, J. Yang, S.J. Lou, Converter slag–coal cinder columns for the removal of phosphorous and other pollutants, *J. Hazard. Mater.* 168 (2009) 331–337.
- [16] M. Achak, L. Mandi, N. Ouazzani, Removal of organic pollutants and nutrients from olive mill wastewater by a sand filter, *J. Environ. Manage.* 90 (2009) 2771–2779.
- [17] N. Selvaraju, S. Pushpavanam, Adsorption characteristics on sand and brick beds, *Chem. Eng. J.* 147 (2009) 130–138.
- [18] X.H. Guan, G.H. Chen, C. Shang, Adsorption behavior of condensed phosphate on aluminum hydroxide, *J. Environ. Sci.* 19 (2007) 312–318.
- [19] X.F. Yang, D.S. Wang, Z.X. Sun, H.X. Tang, Adsorption of phosphate at the aluminum (hydr)oxides–water interface: role of the surface acid–base properties, *Colloids Surf. A* 297 (2007) 84–90.
- [20] N. Kawasaki, F. Ogata, H. Tominaga, Selective adsorption behavior of phosphate onto aluminum hydroxide gel, *J. Hazard. Mater.* 181 (2010) 574–579.
- [21] L. Zeng, X.M. Li, J.D. Liu, Adsorptive removal of phosphate from aqueous solutions using iron oxide tailings, *Water Res.* 38 (2004) 1318–1326.
- [22] J.A. Rentz, I.P. Turner, J.L. Ullman, Removal of phosphorus from solution using biogenic iron oxides, *Water Res.* 43 (2009) 2009–2035.
- [23] H.Y. Wu, D.H. Jiang, P. Cai, X.G. Rong, Q.Y. Huang, Effects of low-molecular-weight organic ligands and phosphate on adsorption of *Pseudomonas putida* by clay minerals and iron oxide, *Colloids Surf. B* 82 (2011) 147–151.
- [24] D.C. Southam, T.W. Lewis, A.J. McFarlane, J.H. Johnston, Amorphous calcium silicate as a chemisorbent for phosphate, *Curr. Appl. Phys.* 4 (2004) 355–358.
- [25] M. Khadhraoui, T. Watanabe, M. Kuroda, The effect of the physical structure of a porous Ca-based sorbent on its phosphorus removal capacity, *Water Res.* 36 (2002) 3711–3718.
- [26] L.A. Rodrigues, M.L.C.P.D. Silva, Thermodynamic and kinetic investigations of phosphate adsorption onto hydrous niobium oxide prepared by homogeneous solution method, *Desalination* 263 (2010) 29–35.
- [27] J.B. Xiong, Q. Mahmood, Adsorptive removal of phosphate from aqueous media by peat, *Desalination* 259 (2010) 59–64.
- [28] H.L. Liu, X.F. Sun, C.Q. Yin, C. Hu, Removal of phosphate by mesoporous  $ZrO_2$ , *J. Hazard. Mater.* 151 (2008) 616–622.
- [29] R. Chitrakar, S. Tezuka, A. Sonoda, K. Sakane, K. Ooi, T. Hirotsu, Selective adsorption of phosphate from seawater and wastewater by amorphous zirconium hydroxide, *J. Colloid Interface Sci.* 297 (2006) 426–433.
- [30] Y.M. Zheng, S.F. Lim, J.P. Chen, Preparation and characterization of zirconium-based magnetic sorbent for arsenate removal, *J. Colloid Interface Sci.* 338 (2009) 22–29.
- [31] B.K. Biswas, K. Inoue, K.N. Ghimire, H. Harada, K. Ohto, H. Kawakita, Removal and recovery of phosphorus from water by means of adsorption onto orange waste gel loaded with zirconium, *Bioresour. Technol.* 99 (2008) 8685–8690.
- [32] Y. Zhang, H. Wang, B. Yan, Y.W. Zhang, J.S. Li, G.L. Shen, R.Q. Yu, A reusable piezoelectric immunosensor using antibody-adsorbed magnetic nanocomposite, *J. Immunol. Methods* 332 (2008) 103–111.
- [33] Y.M. Ren, M.L. Zhang, D. Zhao, Synthesis and properties of magnetic Cu(II) ion imprinted composite adsorbent for selective removal of copper, *Desalination* 228 (2008) 135–149.
- [34] Q.Z. Guo, B. Mei, S.X. Zhou, Z.G. Shi, Y.Q. Feng, J.Y. Wu, G.P. Yan, L. Li, Synthesis, characterization and application of magnetic-zirconia nanocomposites, *J. Non-Cryst. Solids* 355 (2009) 922–925.
- [35] Y. Feng, J.L. Gong, G.M. Zeng, Q.Y. Niu, H.Y. Zhang, C.G. Niu, J.H. Deng, M. Yan, Adsorption of Cd(II) and Zn(II) from aqueous solutions using magnetic hydroxypatite nanoparticles as adsorbents, *Chem. Eng. J.* 162 (2010) 487–494.
- [36] H.Y. Zhu, R. Jiang, L. Xiao, W. Li, A novel magnetically separable  $\gamma$ - $Fe_2O_3$ /crosslinked chitosan adsorbent: preparation, characterization and adsorption application for removal of hazardous azo dye, *J. Hazard. Mater.* 179 (2010) 251–257.
- [37] Y. Li, X.F. Yin, F.R. Chen, H.H. Yang, Z.X. Zhuang, X.R. Wang, Synthesis of magnetic molecularly imprinted polymer nanowires using a nanoporous alumina template, *Macromolecules* 39 (2006) 4497–4499.
- [38] S.K. Apte, S.D. Naik, R.S. Sonawane, B.B. Kale, Synthesis of nanosize-necked structure  $\alpha$ - and  $\gamma$ - $Fe_2O_3$  and its photocatalytic activity, *J. Am. Ceram. Soc.* 90 (2007) 412–414.
- [39] F.C. Wu, R.L. Tseng, R.S. Juang, Enhanced abilities of highly swollen chitosan beads for color removal and tyrosinase immobilization, *J. Hazard. Mater.* B 81 (2001) 167–177.
- [40] G. McKay, The adsorption of dyestuffs from aqueous solutions using activated carbon. III. Intraparticle diffusion processes, *J. Chem. Tech. Biotechnol.* 33A (1983) 196–204.
- [41] H. Li, J.Y. Ru, W. Yin, X.H. Liu, J.Q. Wang, W.D. Zhang, Removal of phosphate from polluted water by lanthanum doped vesuvianite, *J. Hazard. Mater.* 168 (2009) 326–330.
- [42] G.S. Zhang, H.J. Liu, R.Q. Liu, J.H. Qu, Removal of phosphate from water by a Fe–Mn binary oxide adsorbent, *J. Colloid Interface Sci.* 335 (2009) 168–174.
- [43] R. Chitrakar, S. Tezuka, A. Sonoda, K. Sakane, K. Ooi, T. Hirotsu, Adsorption of phosphate from seawater on calcined MgMn-layered double hydroxides, *J. Colloid Interface Sci.* 290 (2005) 45–51.
- [44] S.L. Tian, P.X. Jiang, P. Ning, Y.H. Su, Enhanced adsorption removal of phosphate from water by mixed lanthanum/aluminum pillared montmorillonite, *Chem. Eng. J.* 151 (2009) 141–148.